

Bilirubin Biosensing by Using of Catalase and ZnS Nanoparticles as Modifier

Hamideh Dehghani¹, Shahrzad Khoramnejadian², Mohammad Mahboubi³, Masoomeh Sasani², Samira Ghobadzadeh⁴, Saghar Mowlazadeh Haghighi⁵, Masoud Negahdary^{6,*}

¹Department of Nursing, Shahid Sadoughi University of Medical Sciences, Yazd, Iran

²Department of Environment, Damavand branch, Islamic Azad University, Damavand, Iran

³Abadan School of Medical Sciences, Abadan, Iran

⁴Department of Immunology, Faculty of Medical Sciences, Tarbiat Modares University, Tehran, Iran

⁵Department of Chemistry and Biochemistry, University of Arizona 1306 E, University Blvd, Tucson, AZ 85721, USA

⁶Young Researchers and Elite Club, Marvdasht Branch, Islamic Azad University, Marvdasht, Iran

*E-mail: Masoudnegahdary@ssu.ac.ir

Received: 1 October 2015 / Accepted: 31 December 2015 / Published: 1 February 2016

To find a stable bilirubin biosensor we used of catalase and ZnS nanoparticles (Nps); the detection of bilirubin in this research designed on Bioelectrochemical measurement cyclic voltammetry (CV) techniques. ZnS Nanoparticles synthesized and investigated by X-Ray diffraction (XRD), UV-Visible (UV-VIS) and scanning electron microscopy (SEM). The redox peaks studied in the range of +0.5 to -0.5 V and formal potential (E^0) calculated as 40 mV; also $\Delta E_p = 70$ mV. In this research the anodic peak current of showed a linear relationship for different concentrations of bilirubin in the range of 3 to 50 μM . The linear equation was expressed as $i_{pa} (\mu\text{A}) = -0.1417 - 0.3661(\mu\text{M})$ ($R^2 = 0.9885$) with a detection limit of 2 μM for this research. The optimum pH effect was 7.0 and maximum temperature response was around 25 °C. Interference agents not showed a significant effect on this bilirubin biosensor.

Keywords: Bilirubin, ZnS nanoparticles, Catalase, Biosensing

1. INTRODUCTION

Bilirubin is compound creates in gall, a liquid made by the liver. Bilirubin (previously mentioned to as haematoidin) is manufactured by heme catabolism, affected by the body's purging of old red blood cells that have hemoglobin [1, 2]. In the liver, bilirubin interacts with sugars to produce a hydrophilic form named conjugated bilirubin [3]. Conjugated bilirubin cross from the liver, and in the large intestine, it is reconverted to the unconjugated bilirubin en route to being excreted from the body

[4]. Researches showed that bilirubin produced by the action of reductase against biliverdin, a tetrapyrrolic bile pigment that is as well as a product of heme degradation [5]. When the oxidation occurred for bilirubin, once again it returns convert to biliverdin. Hyperbilirubinemia defined as outcomes from a higher-than-normal volume of bilirubin in the blood. For the adult the level above 17 $\mu\text{mol/l}$ and for babies 340 $\mu\text{mol/l}$ and serious hyperbilirubinemia 425 $\mu\text{mol/l}$ defined. Progress electrochemical methods along with making electrochemical biosensors are essential in this research fields. Hyperbilirubinemia lead to Physiological jaundice, hemolytic jaundice, Gilbert's disease, Crigler-Najjar syndrome, Dubin-Johnson syndrome and biliary obstruction [6-9]. Also Hypobilirubinemia perhaps be a probable risk factor of end-stage kidney disease (ESKD) [10]. According to importance level of bilirubin, find a new approach to detect it is necessary [11]. Biosensing provided a novel, exact, fast and cheap way to determination of biochemical compounds (analytes) [12-14]. Bilirubin is also a target analyte for biosensors [15-18]. Usually electrochemical methods involved in all designed biosensors. Significant levels of publicized work on the enzyme-based biosensors are normally found from the literature [19-21]. Pursuant to medical applications, industrial availableness and exclusive properties, heme enzymes were applied in many biosensors to detect analyte [22-24]. Some bilirubin biosensors designed before [15-18]. Here also we prepared an enzyme based (catalase) bilirubin biosensor. Catalase participate in a haemeo transfer mechanism and this mechanism used for Bioelectrochemical studies [25-27]. ZnS nanoparticles could maybe be used as good catalysts and as a result of nanotechnology on the direct electron transfer [28, 29]; we used of this nanoparticles as Bioelectrochemical facilitator. The quantum effects of nanoparticles improves the band gap of their catalysts properties to improvement the particular redox actions [30, 31]. Currently many types of nanoparticles used in biosensors [32, 33]. Here, we investigated biosensing and determination of bilirubin by using of catalase (EC 1.11.1.6) and modified carbon paste electrode with Zns nanoparticles and their potential applications as biosensors and their use as suitable templates for determination of bilirubin.

2. EXPERIMENTAL

2.1. Reagents and materials

Bilirubin (Linear Formula: $\text{C}_{33}\text{H}_{36}\text{N}_4\text{O}_6$), Catalase from human erythrocytes, Polyvinylpyrrolidone, Polyvinyl alcohol, Polyethylene glycol, Zinc acetate dehydrate, Sodium sulfide, Mineral oil Bio Ultra, sodium hydroxide, and Tris HCl buffer purchased from Sigma Aldrich (USA). Carbon powder has been purchased from Superior Graphite (Sweden). Other reagents provided by certified Iranian chemical companies. Phosphate buffer solution (PBS), 0.1 M, pH 7.0 was prepared from anhydrous disodium hydrogen phosphate (Na_2HPO_4) and sodium dihydrogen phosphate (NaH_2PO_4). Deionized water was used for aqueous solution preparations. Analytical grade argon (Afrox, South Africa) was used to degas the system. All experiments were done in room temperature (25°C).

2.2. Apparatus and analytical methods

Electrochemical measurements were being accomplished with a computer-controlled-Autolab modular electrochemical method (Eco Chemie Ultecht, The Netherlands), influenced using GPES application (Eco Chemie). All electrochemical experiments were being conducted having a conventional a three electrode system with a fabricated CPE (diameter, 3mm) as the working electrode, Ag/AgCl as the reference electrode (Gamry Instruments, USA), and a platinum as counter electrode (Gamry Instruments, USA). The absorption spectra of ZnS nanoparticles were recorded with an UV-Visible spectrophotometer (UV-3600 series, Kyoto, Japan) in the range of 200-800 nm. X-ray diffraction (XRD) of ZnS nanoparticles was carried out on X'pert Pro X-ray diffractometer (Panalytical B.V., Netherlands) operating at 40 kV to determine the ZnS nano crystalline phase and structure. The size and morphology of the nanoparticles were investigated by SU3500 Premium VP-SEM Scanning Electron Microscopes (SEM) (Japan).

2.3. Preparation of ZnS nanoparticles

ZnS Nanoparticles have been synthesized making use of PVP, PVA and PEG-4000 because capping agencies by straightforward co-precipitation technique [34]. The particular theory involved in this technique could be the precipitation associated with precious metal ions with sulfide ions inside solution [35]. The 0.1 M aqueous solution associated with Zinc acetate di hydrate and 0.1 M aqueous solution associated with Sodium sulfide have been mixed in the presence of various capping agent solutions like PVP, PVA and PEG-4000. solutions of 0.1 M Zinc acetate di hydrate, 0.1M Sodium sulfide and 1% by weight of capping agents were prepared in two times distilled water. the 15 ml associated with zinc acetate and 15 ml associated with 1% associated with PVP have been mixed with each other and stirred for half an hour over a magnetic stirrer to get a homogeneous solution. This is accompanied by drop wise addition associated with proper volume of 0.1 M Sodium sulfide within healthy vigorous intended for 1 hour. The light colour precipitate seemed to be acquired that is lost by simply centrifugation in addition to laundered once or twice together with dual distilled water. The precipitate seemed to be dried out throughout the oven with 80°C intended for 4 hours to obtain powder sample. While using very same approach, ZnS Nanoparticles had been organized applying other capping agencies in addition.

2.4. Preparation unmodified carbon paste electrode (CPE)

Unmodified CPE had been cooked by hand-mixing carbon powder as well as mineral oil with the 80: 20 (w/w) relations. the achieved paste had been very carefully put together as well as homogenized in a agate mortar pertaining to 20 min. the producing paste had been stored in area temperatures inside a desiccator just before make use of it. The paste has been stuffed strongly in to a cavity (3.6 mm diameter as well as 2 mm depth) at the end of a Teflon tube. Electric contact has been recognized by a copper wire linked to the paste inside the inner hole of the tube. The electrode surface

had been lightly smoothed by means of weighing paper before use. This process had been furthermore employed to regenerate the surface of CPE.

2.5. Preparation modified carbon paste electrode with ZnS nanoparticles

The ZnS nanoparticles modified CPE were prepared by mixing carbon powder, mineral oil, and ZnS nanoparticles with ratios of 60:20:20 (w/w/w) in an agate mortar until a uniform paste was obtained. The paste gained in this method was filled into the hole at the end of the Teflon tube; other next steps were repeated as preparation unmodified carbon paste electrode.

2.6. Preparation modified carbon paste electrode with ZnS nanoparticles and Catalase

The modified carbon paste electrode with ZnS nanoparticles and Catalase were prepared by a simple drop-cast coating method (3 μ l of 10 mg/ml) on surface of working electrode and permitted to dry for 2 hour at room temperature under clean location. After drying these products were washed by dipping in 0.1M PBS (pH 7.0) to remove nonimmobilized enzyme and boundless ZnS nanoparticles from probe and were kept at 4°C till use.

2.7. Bilirubin biosensor procedure

The purchased bilirubin (Molecular Weight 584.678) was prepared according to sigma Co instructions as below: A 0.002% aqueous solution is first prepared by suspending 1 mg bilirubin in 1 ml of water. Approximately 1 drop of 2 M sodium hydroxide is added to dissolve the product before bringing to a final volume of 50 ml with 200 mM Tris HCl, pH 8.4. In electrochemical studies for bilirubin detection, the prepared aqueous were added to the electrochemical cell by dropping with exact concentrations.

3. RESULTS AND DISCUSSION

3.1. X-Ray diffraction study of synthesized ZnS nanoparticles

The x-ray diffraction records were documented by expending Cu K α radiation (1.5406 Å). The intensity records were composed over a 2 θ range of 20-80°. To find the average particles size, the samples was assessed with the use of Scherrer equation via the diffraction intensity of peak [36, 37]. All X- ray diffraction trainings approved that the synthesized agents were ZnS with wurtzite.

$$D=0.89\lambda / (\beta \text{ Cos } \theta) \quad (1)$$

In this equation the λ is the wavelength (Cu K α), β is the full width at the half-maximum (FWHM) of the ZnS (101) line and θ is the diffraction angle. The crystal-like nature of the synthesized

ZnS nanoparticles is proved from the x-ray diffraction pattern. The maximum important feature in the observed pattern, at $2\theta=27.5634$, is assigned to the (111) reflection of the cubic zinc blende structure of ZnS (JCPDS No 5-566) [38]. Two other leading features are detected at $2\theta = 46.5321$ and 55.3412 , which belong to (220) and (311) reflections. An explicit series broadening in the diffraction peaks is definitely an indicator the synthesized ZnS nanoparticles will be in nanometer scale [39]. This grate boundaries worked out has been furthermore with deal using the reported values (figure 1).

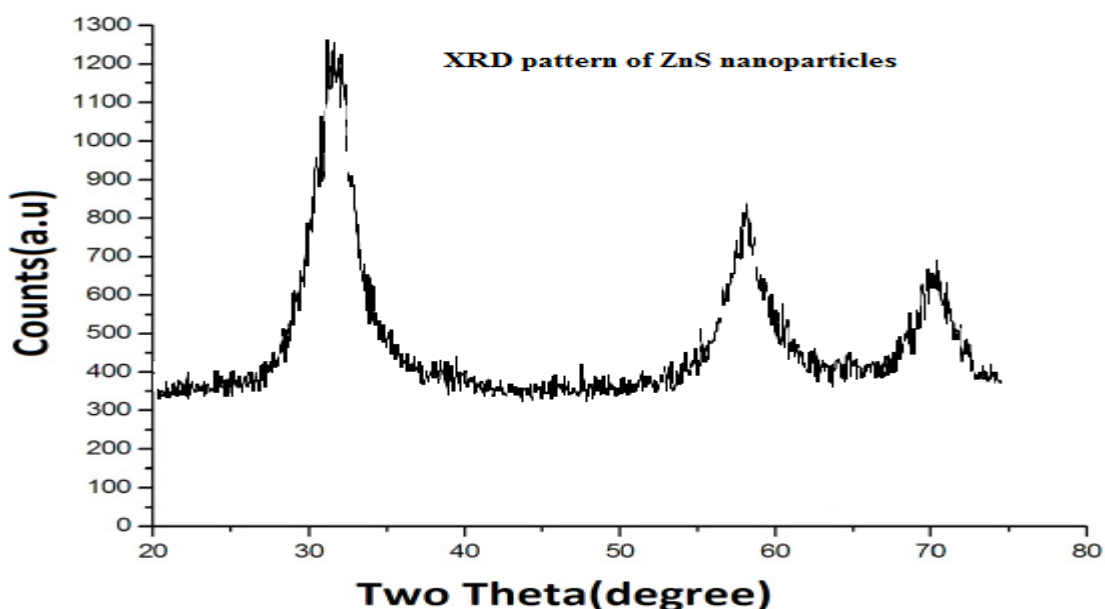


Figure 1. X-Ray diffraction of synthesized ZnS nanoparticles

3.2. Ultra Violet Visible (UV-VIS) spectroscopy of ZnS nanoparticles

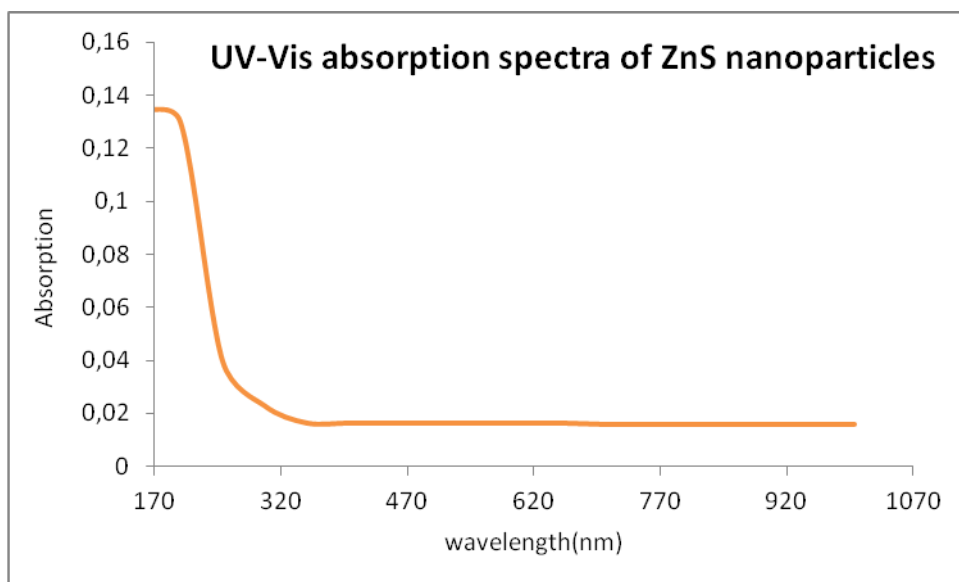


Figure 2. UV-VIS spectroscopy of ZnS nanoparticles

UV-visible spectroscopy is generally one of the utilized methods for structural characterization of metal nanoparticles [40-42]. These nanoparticles display a solid UV-Vis absorption band that is not existing in the band of the bulk metal. The UV-Vis spectral range is about 190 to 900 nm, as provided by the applicable range of usual commercial UV-VIS devices. Figure 2 indicates the particular UV-visible absorption spectra of ZnS nanoparticles at the room temperature (25 C°) state. These spectra exhibited UV absorption shift peak at 205 nm showing a mono dispersed size of particles. The linear part indicated that the approach of shift in this material is of direct nature. The band gap energy in a nanomaterial could be achieved from the absorption greatest [43, 44]. Based on quantum confinement model, electrons are in the transfer band group [45, 46]. The shoulder or peak of the spectra relates to the essential absorption edges in the samples, and could be used to evaluate the band gap of the nanoparticles.

3.3. Scanning electron microscopy (SEM) & size distribution of ZnS nanoparticles

The SEM is regularly used to produce high quality images and to display three-dimensional variants in chemical structures [47]. The SEM is also commonly used to detect phases based on qualitative chemical analysis and/or crystalline structure. Exact measurement of very small features and objects down to 50 nm in size is also accomplished using the SEM [48]. Here we investigated morphology of ZnS nanoparticles by an SEM and with scale bar 20 nm (figure 3 (a)). Also the particle-size distribution histogram of ZnS nanoparticles determined and exhibited (figure 3 (b)). An agglomeration of nanoscale particles is evidently detected, showing a uniform distribution of particle size and a similar morphology.

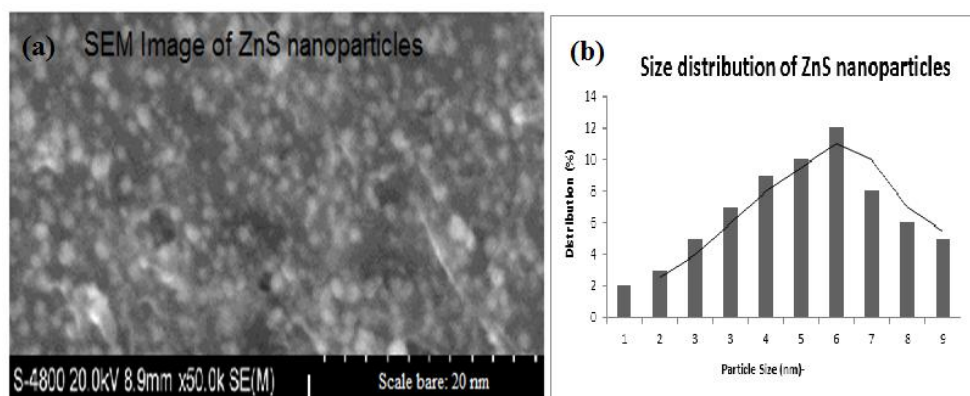


Figure 3. (a): SEM image of ZnS nanoparticles, (b): size distribution of ZnS nanoparticles

3.4. Direct electrochemistry of catalase immobilized on modified carbon paste electrode with ZnS nanoparticles

Figure 4 presented the typical CVs of different electrodes state in 0.1 M pH 7.0 PBS at a scan rate of 50 mV s⁻¹. As shown, no redox peaks were observed at bare CPE which indicated that neither CPE was electroactive species in the examined range (figure 4 (a)). In the catalase-CPE, a weak redox

peak was observed (figure 4 (b)), but CPE/Catalase/ZnS Nps gave an enhancing redox peak in the range of +0.5 to -0.5 V. It was noteworthy that a pair of well-defined and reversible redox peaks was observed at CPE/Catalase/ZnS Nps (figure 4 (c)). The anodic and cathodic peak potentials were located at 75 mv and 5 mv with the formal potential ($E^{\circ} = (E_{pc} + E_{pa})/2$) 40 mv. The CPE/Catalase/ZnS Nps showed a well-defined redox couple with a peak to peak separation ($\Delta E_p = E_{pa} - E_{pc}$) of 70 mV at scan rate of 50 mV s^{-1} . The ΔE_p value indicates a reversible and fast electron transfer process.

$$\Delta E_p = 0.058/n$$

$$(\Delta E_p = E_{pa} - E_{pc}) = 70 \text{ mV}$$

$$n = 0.82 \approx 1 \text{ electron transfer}$$

The obtained results indicated that catalase was successfully confined to the electrode surface, and the direct electron transfer of catalase was achieved through the important role of ZnS nanoparticles. The reason may be as follows: excellent ability in acceleration of electron transfer. More importantly, the structure of the ZnS nanoparticles with high surface area played an important role in the immobilization of catalase through absorption. Meanwhile, ZnS nanoparticles deposited on the surface of carbon paste electrode as electron transfer facilitator bridges or connectors between those neighboring catalase molecules and electrode surface, and shortened the distance of electron transfer, which was benefit to the facilitating the electron transfer of catalase. Therefore, ZnS nanoparticles can provide more sites and channels for the immobilization of catalase, aiding in the prevention of the denaturation and leakage of catalase, and enhancing the electron conductivity [49, 50].

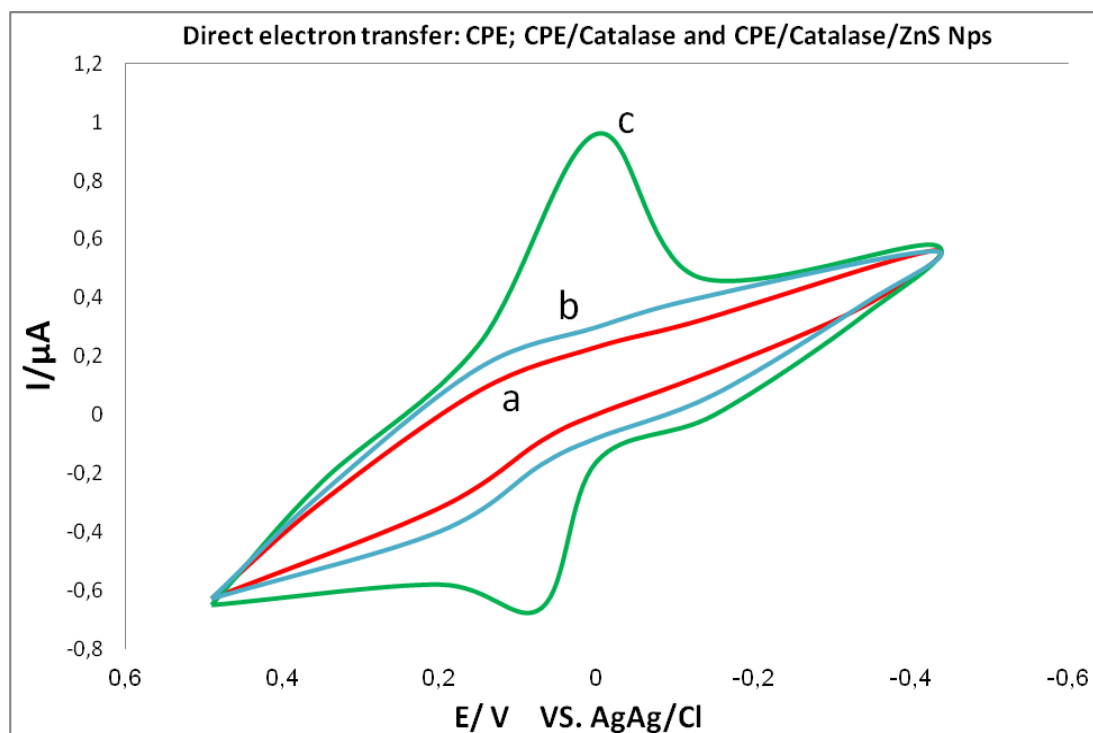


Figure 4. Cyclic voltammograms of (a) bare CPE, (b) CPE/Catalase and (c) CPE/Catalase/ZnS Nps, Phosphate buffer solution (PBS): 0.1 M pH 7.0, scan rate: 50 mV s^{-1} .

3.5. Effect of various scan rates on catalase immobilized on modified carbon paste electrode with ZnS nanoparticles

Figure 5 shows the CVs of the CPE/Catalase/ZnS Nps recorded in 0.1 mol L⁻¹ PBS (pH 7.0). The influence of scan rate on the response of the CPE/Catalase/ZnS Nps in 0.1 M pH 7.0 PBS was investigated. As shown in Figure 5, it was found that both anodic and cathodic peak currents increased clearly with the increase of the scan rate.

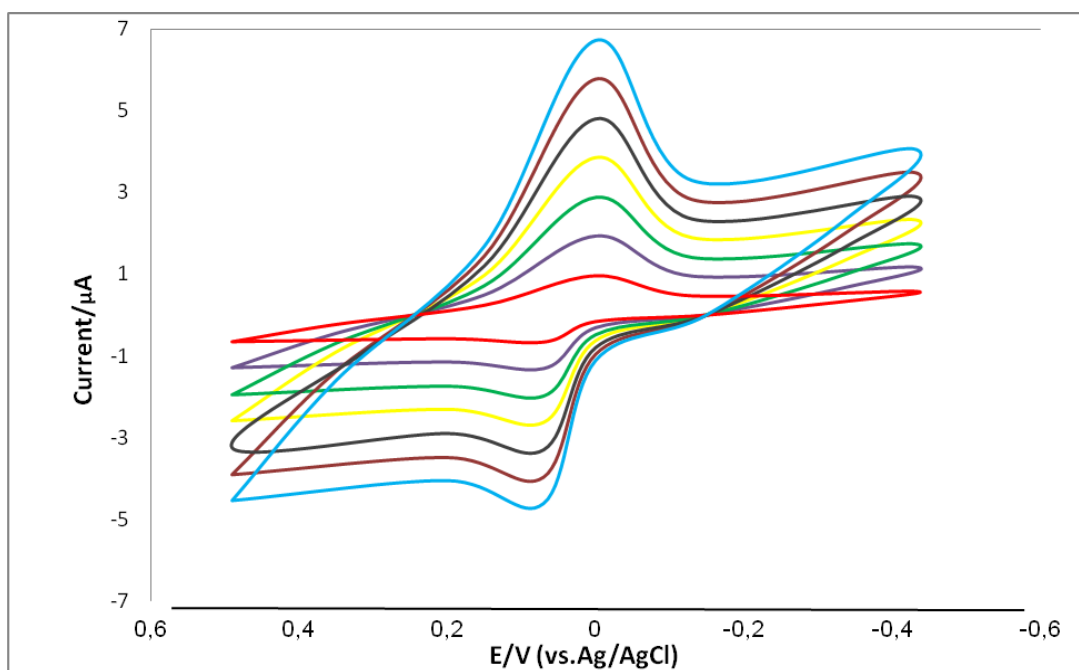


Figure 5. Cyclic voltammograms of Catalase immobilized CPE/ZnS Nps at the different scan rates, from: 50, 100, 150, 200, 250, 300 and 350 mVs⁻¹. Phosphate buffer solution (PBS): 0.1 M pH 7.0

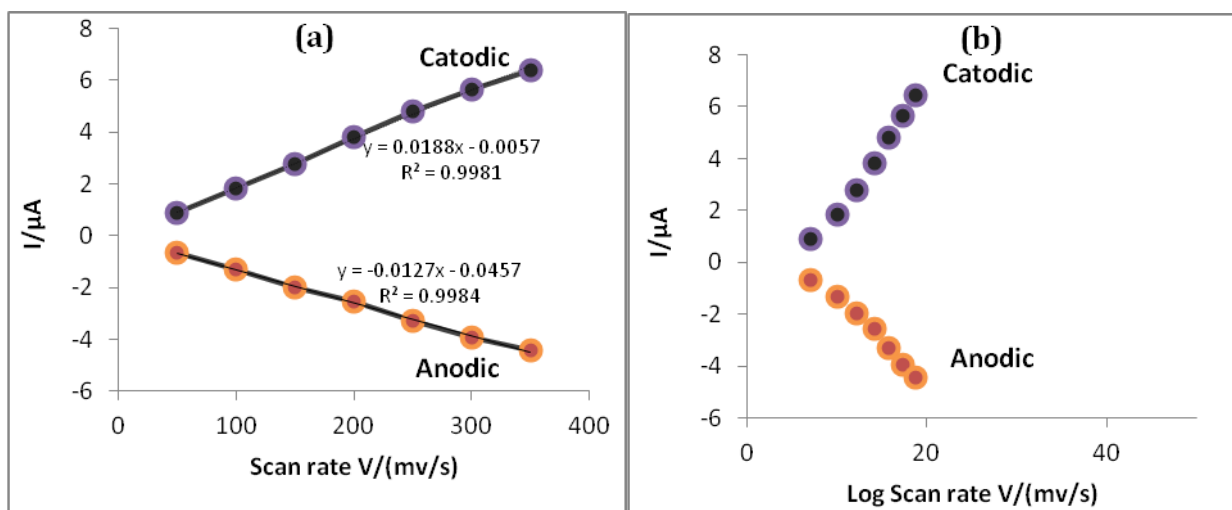


Figure 6. Linearly relationship between anodic and cathodic peak (a): VS. Scan rate and (b): Versus. X^{1/2}, Phosphate buffer solution (PBS): 0.1 M pH 7.0

The currents of peak remained linearly linked to the scan rate (figure 6 (a)) and furthermore square root of the scan rate in the range from 50 to 350 mVs^{-1} (figure 6 (b)); showing a good bioelectrochemical redox behavior and this phenomena was found in previous studies also [51-54]. The linear regression equation was $I_{pa} y = -0.0127x - 0.0457$, $R^2 = 0.9984$ ($n=1$) and $I_{pc} y = 0.0188x - 0.0057$, $R^2 = 0.9981$ ($n=1$), indicating the bioelectrochemical kinetics existed with a good redox reaction [55].

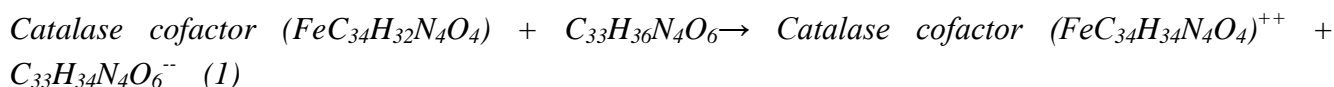
For the bilirubin sensing mechanism based on an enzymatic reaction catalyzed by catalase; the electromotive force (EMF) response of ion selective electrodes, the glucose biosensor, can be explained according to Nernst's expression:

$$E = E^{\circ} + 2.3 \frac{RT}{nF} \text{Log} \left(\frac{\text{OX}}{\text{Red}} \right) \quad (1)$$

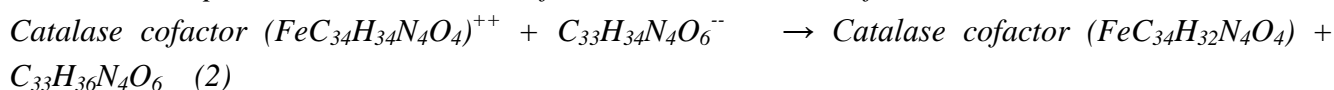
where E is the cell potential at some moment in time, E° is the cell potential when the reaction is at standard-state conditions, R is the ideal gas constant in units of Joules per mole, T is the temperature in Kelvin, Faraday constant ($F = 96493 \text{ C/mol}$) n is the number of moles of electrons transferred in the balanced equation for the reaction, and F is the charge on a mole of electrons. The apparent heterogeneous electron transfer rate constant (k_s) of Catalase immobilized CPE/ZnS Nps is calculated from Laviron equation 1 (for $n \Delta E_p < 200$) [56]:

$$k_s = \frac{(1 - \alpha)nFV}{\frac{RT}{\alpha(1 - \alpha)F}}$$

Where α is the charge transfer coefficient is assumed ≈ 0.9 and n is the transferred electrons number is assumed 1. ΔE_p is the peak separation of the Catalase redox couple obtained 70 mV at scan rate of 50 mV s^{-1} , T is the room temperature (298.15 K) and R is the universal gas constant ($8.314 \text{ J mol}^{-1} \text{ K}^{-1}$). Based on Laviron theory, the electron transfer rate constant (K_s) and charge transfer coefficient (α) can be determined by measuring the variation of peak potential with scan rate [57]. The calculated rate constant (k_s) for electron transfer of Catalase at Catalase immobilized CPE/ZnS Nps is 1.94 s^{-1} , indicating fast electron transfer process. A schematic structure of designed bilirubin biosensor with three important elements showed at figure 7. All sections in figure 8 (a-d) show relevant mechanism of this bilirubin biosensor. The molecular structure of catalase and bilirubin shown at figure 8 (a & b) respectively. The redox reaction occurred between them and bilirubin oxidized to biliverdin. In this electrochemical reaction catalase reduced. The active site of catalase and heme of it has been showed at figure 8 (c); also the biliverdin molecular structure shown at figure 8 (d). The recommended mechanism in this biosensor cited as reactions (1-2):



Mechanism output results: 1. Reduction of catalase, 2. Oxidation of bilirubin to biliverdin



Mechanism output results: 1. Oxidation of catalase, 2. Reduction of biliverdin to bilirubin

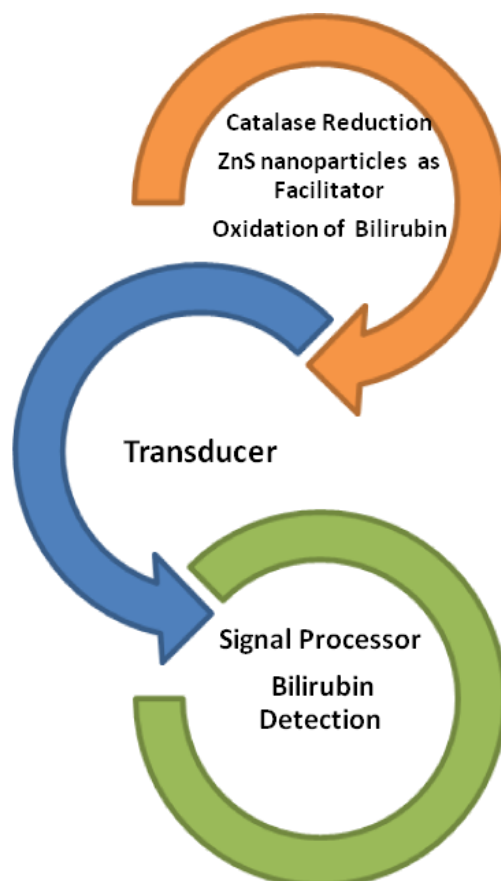
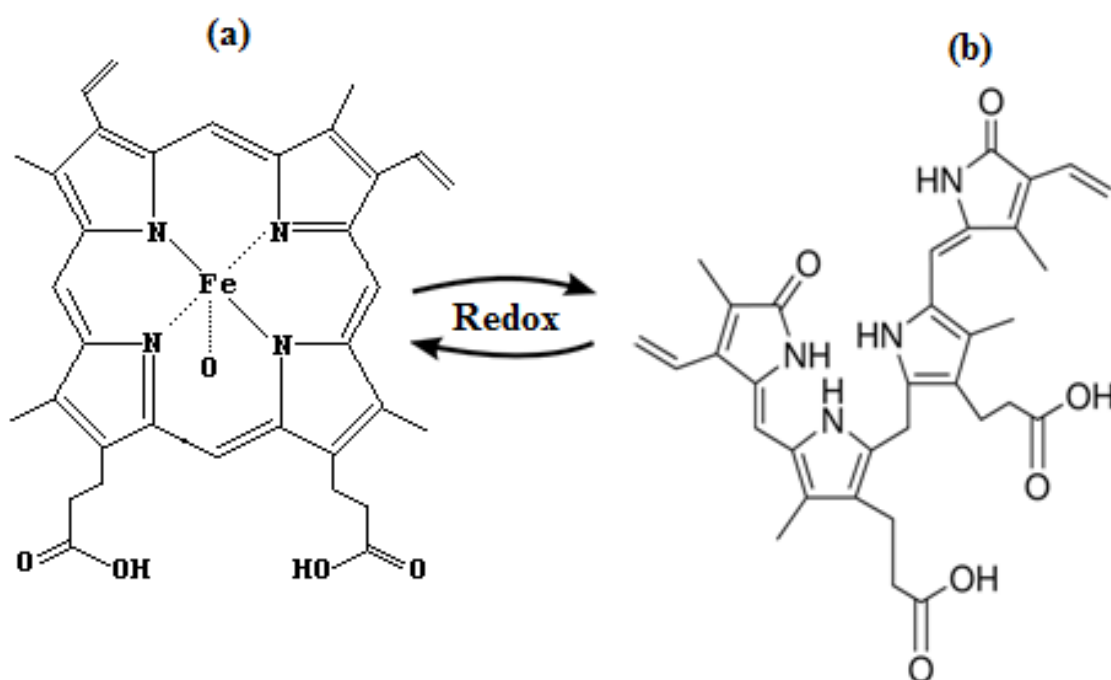


Figure 7. Schematic structure of designed bilirubin biosensor



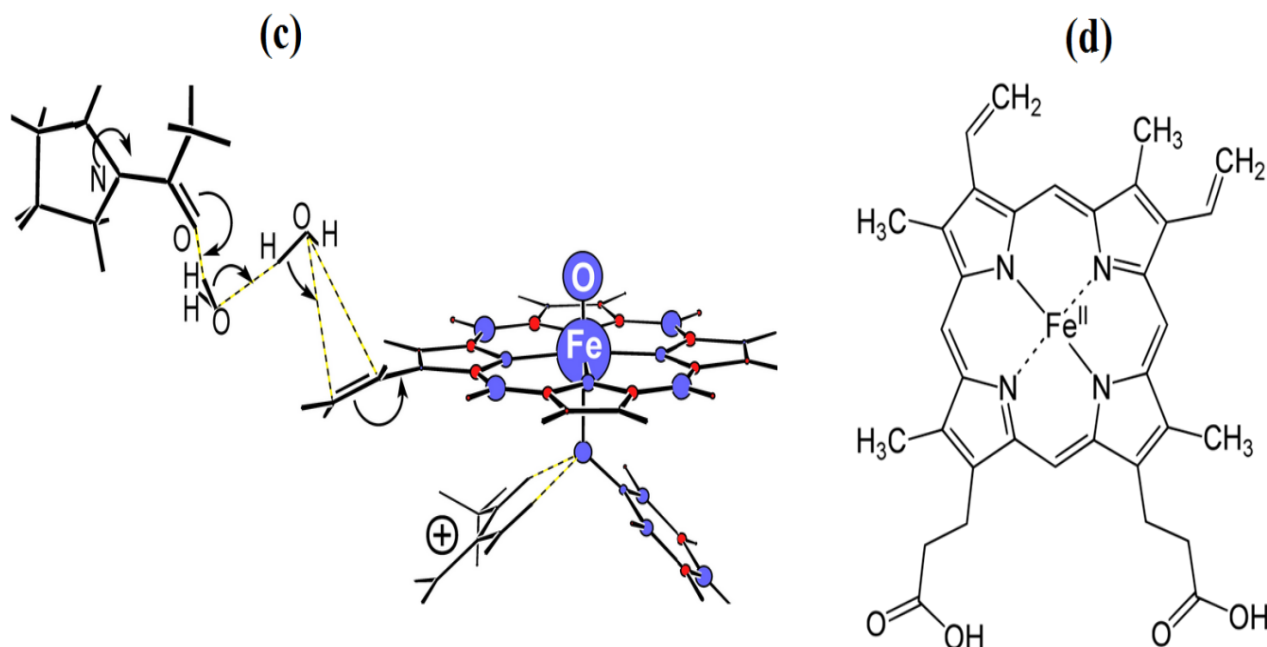


Figure 8. (a): molecular structure of catalase, (b): molecular structure of bilirubin, (c): active site of catalase & heme, (d): molecular structure of biliverdin

An rise in the current or a alteration in the reaction potential to additional facile direction for an electrochemical reaction saw on a modified electrode surface is so called the electrocatalytic effect of the modifier [58, 59]. To follow analyte detect, the cyclic voltammograms for a series of standard bilirubin solutions were recorded in an electrochemical cell contained PBS (0.1 M and pH 7.0) studied using the proposed biosensor (CPE/Catalase/ZnS Nps). As shown in Figure 10 (a) the current signal intensity due to the oxidation of bilirubin which is started at about 100 mV versus Ag/AgCl electrode decreases with increasing the concentration of bilirubin. Figure (9 a) shows that anodic current rises with successive addition of bilirubin. Differences of the oxidation peak current of bilirubin (i_{pa}) as a purpose of the potential scan rate (v) showed a linear performance upon addition of various concentrations of bilirubin; this outcome demonstrating that the charge transfer rate at the catalase immobilized CPE/ZnS Nps electrode surface is controlled by the redox reaction of bilirubin adsorbed on the surface. This performance is used in this research to improve a way for fast detection of bilirubin based on anodic adsorptive voltammetry. It was observed that the peak currents enhanced greatly at ZnS nanoparticles modified CPE, which provides high surface area of the ZnS nanoparticles improved the electrode contacting area of bilirubin and its electrochemistry of reaction product, which increased. The result showed that the electron transfer reaction was controlled by diffusion and increases in the concentrations of bilirubin. In this research the anodic peak current of bilirubin showed a linear relationship for different concentrations of bilirubin (figure 9.b) in the range of 18 to 34 μM . The linear equation was expressed as $i_{pa} (\mu\text{A}) = -0.185x + 0.31(\mu\text{M})$ ($R^2 = 0.9956$) with a detection limit of 2 μM for this research step. We prepared output results of other designed bilirubin biosensor in table 1.

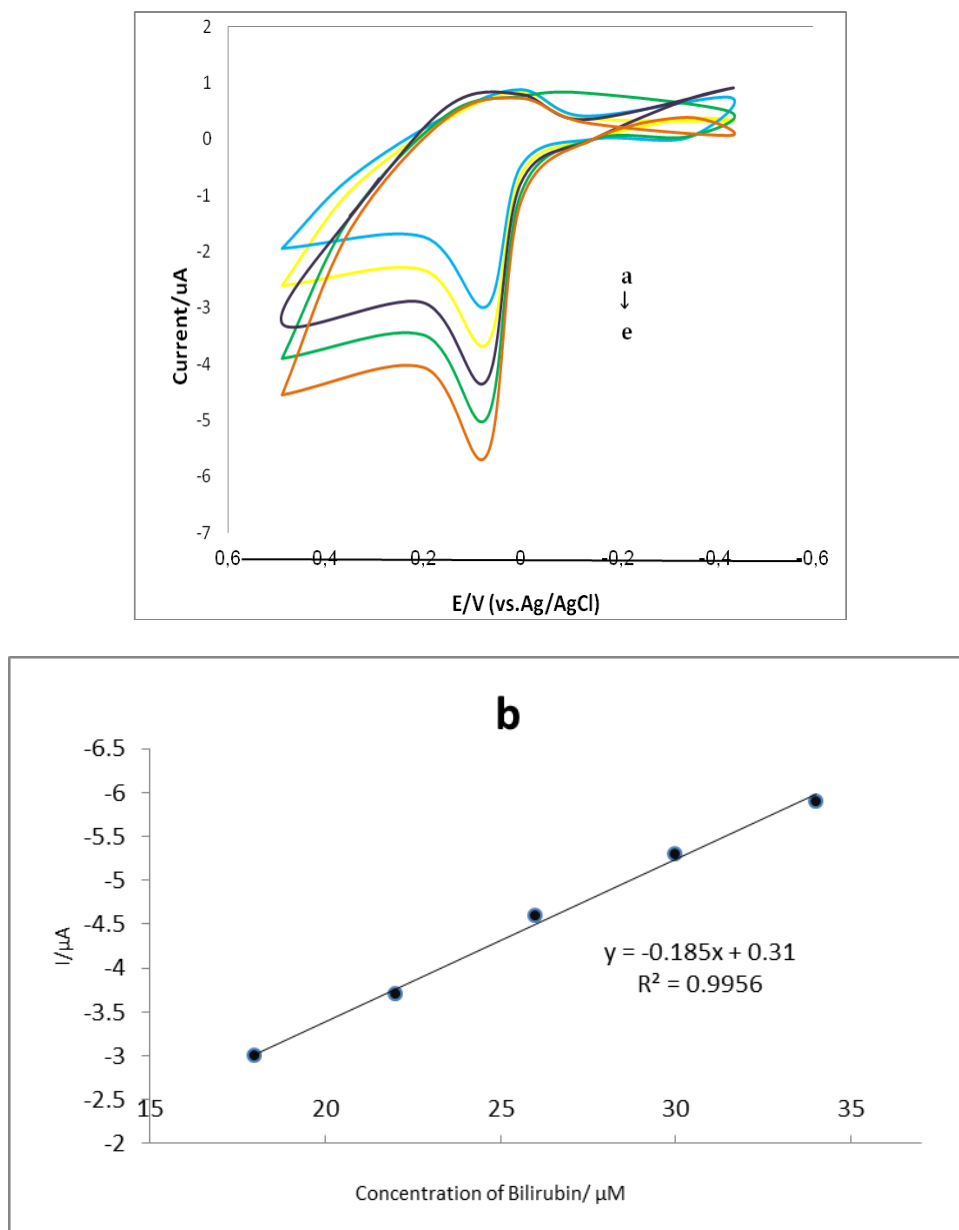


Figure 9. (a) Cyclic voltammograms achieved at an Catalase immobilized CPE/ZnS Nps in 0.1M PBS (pH 7.0) for various concentrations of bilirubin and (b) the correlation among anodic peak current of Catalase and various concentrations of bilirubin (scan rate: 50 mVs^{-1}).

Table 1. Compare elements and determination sensitive to analyte in several bilirubin biosensors

Biosensor elements	Analyte	Linearity	Detection limit	Ref
poly-terthiophene–Mn(II) complex	bilirubin	0.1 μM - 50μM	40±3.8 nM	[60]
Fe2Co coating was electrodeposited on the working microelectrodes	bilirubin	No Reported	56±33 μM	[61]
Screen printed electrodes; Multi-walled carbon nanotubes	bilirubin	200–500 μM	9.4 ± 0.3 μM	[62]
Pyrolyzed Photoresist Carbon Electrodes in Aprotic Solvent	bilirubin	No Reported	No Reported	[63]
Enzymic Method/ Oxygen Electrode	bilirubin	1×10^{-5} - 2.5×10^{-4} M	8×10^{-6} M	[64]

3.6. Effect of pH

investigation of the effect of the pH value on the performance of the biosensor is very importance, because the activity of the immobilized catalase is pH dependent. Enzymes are affected by changes in pH. The maximum conducive pH value - the point where the enzyme is greatest activity - is recognized as the optimum pH. Extraordinary high or low pH amounts commonly lead to complete loss of activity for most enzymes. pH measurement also defined as a cause to examine strength of enzymes. As with activity, for each enzyme there is also a region of pH optimal stability. The influence of pH in PBS: 0.1 M on the peak current of CPE/Catalase/ZnS Nps in the pH range of 3-9 is shown Figure 10 (a). It can be seen that the optimum pH was 7.0. If the pH value was higher or lower than the optimum pH, the peak current for CPE/Catalase/ZnS Nps decreased. For used enzyme (catalase), the optimum pH of 7.0 was selected for following experiments. In other research maximum response for a bilirubin biosensor was obtained at pH 8.5 ± 9.0 [64]. In another research the maximum oxidation current was observed at the pH of 7.0. [60].

3.7. Effect of temperature

Approximately similar to all chemical feedbacks, the level of an enzyme-catalyzed reaction rises as the temperature is raised also [65, 66]. A 10°C rise in temperature lead to progress in the activity of most enzymes by 50 % to 100% [67]. Differences in response temperature as small as 1 or 2 degrees can present variations of 10% to 20% in the outcomes. In the enzymatic reactions, this is complex by the event that numerous enzymes are unfavorably denatured by high temperatures. Like most synthetic responses, the rate of a compound catalyzed response increments as the temperature is raised [65].

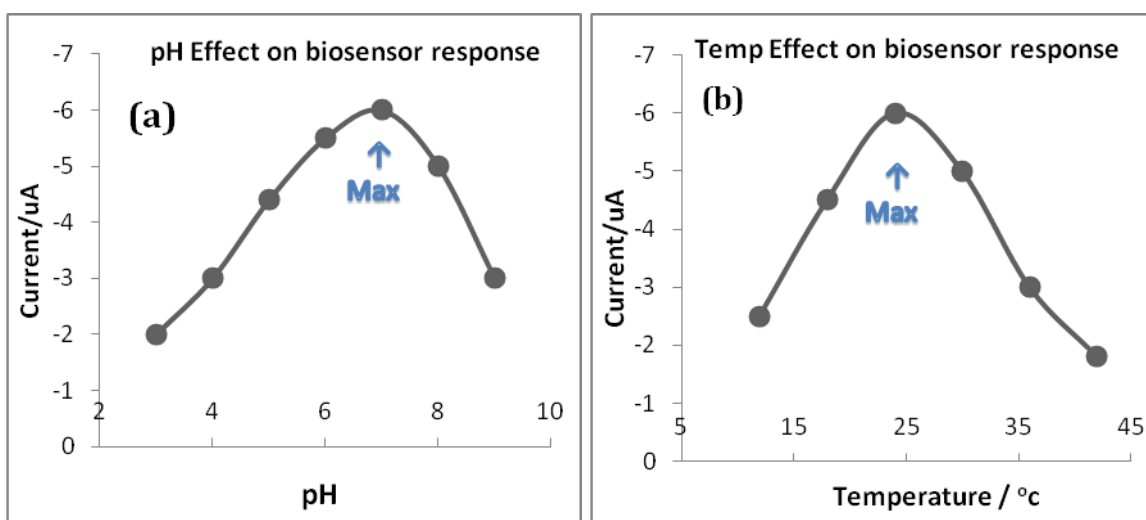


Figure 10. (a) the effect of pH on designed bilirubin biosensor by using of catalase immobilized CPE/ZnS Nps (b) the effect of temperature on designed bilirubin biosensor by using of catalase immobilized CPE/ZnS Nps

Almost all bodily enzymes rapidly become denatured at high temperature (40°C or more) [68]; We studied the activity catalase immobilized CPE/ZnS Nps biosensor, along with the activity of catalase in the temperature range from 12 to 42 °C. The goal was to study the sensitivity of designed bilirubin biosensor based on catalase immobilized CPE/ZnS Nps at various temperatures. The efficiency of the bilirubin biosensor with respect to the temperature can be explained in terms of the optimum temperature at which the biosensor electrode would show the maximum performance. The sensor electrode has shown its maximum response around 25 °C (Figure 10 (b)) which can be attributed to the agitation of ions inside the testing solution with the increase in temperature. Although the optimum temperature for catalase is about 25°C, we did all tests at room temperature due to simplicity of the detection and to avoid any probable evaporation processes. Additionally, the bilirubin biosensor electrode has shown a decreasing potentiometric response above 25 °C due to possible denaturation of the protein molecules at high temperature.

3.8. Constant potential amperometry (CPA) on designed bilirubin biosensor

Constant-potential amperometry is commonly used to find relationships between substrate concentration and biosensor output results [69]. The constant potential amperometry technique offers high sensitivity. This electrochemical assay also passed in this experimental study. CPA is a method where a constant potential, enough to oxidase or reduce the analyte of interest, is used to the electrode and the current is examined [69]. At this research CPA was applied as a technique to calibrate the modified Catalase immobilized CPE/ZnS Nps for bilirubin determination. This involved rotating the working electrode at high speeds till the non-faradaic current had reached a stable level. This produces a step-wise array of time (s) vs. current (μA). The amperometric responses of sequential additions of standard bilirubin was demonstrated in figure 9 (each 2 μM) and tested by Catalase immobilized CPE/ZnS Nps in 0.1 M PBS (pH 7), respectively, rotating speed = 500 rpm. Well-defined stable state current feedback was achieved in 4 s at used potential, and the currents increased stepwise with additions of bilirubin. It could be found linearly dependence between amperometric current and bilirubin concentration during 112–1100 s. The Catalase immobilized CPE/ZnS Nps electrode touched 96% of the stable state current within 10 s (figure 11).

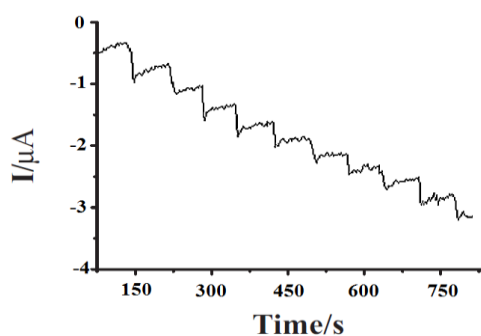


Figure 11. Amperometric responses of bilirubin (each 2 μM) tested by Catalase immobilized CPE/ZnS Nps in 0.1 M PBS (pH 7), rotating speed = 500 rpm

3.9. Interferences

Possible interferences for the detection of bilirubin were investigated by adding various foreign species (ClO_3 , SO_4 , Glycine, Ascorbic acid, Cl^- , Br^-) into the pH 7.0 PBS containing 5 μM bilirubin. The results indicated that these agents had almost no interference. The exact Response change on the determination has been cited in table 2. These potential interferences which may exist in biological samples, The results of this step indicated that this biosensor has high selectivity for bilirubin detection against research of Md. Aminur Rahman et al [60]. The long-term stability of the prepared bilirubin biosensor is a critical factor in practical application [15].

Table 2. Interference of external matters to response of the Catalase immobilized CPE/ZnS Nps to 5. μM bilirubin in 0.1M pH 7.0 PBS

<i>External matters</i>	<i>Concentration spiked (μM)</i>	<i>Response change (%)</i>
ClO_3	30	-1
SO_4	30	2
Glycine	30	4.2
Ascorbic acid	30	3
Cl^-	30	0.7
Br^-	30	-1.3

3.10. Reproducibility and stability of the designed bilirubin biosensor

In order to investigate the designed bilirubin biosensor, a group of voltammetric mensuration was done at the identical Catalase immobilized CPE/ZnS Nps. The relative standard deviation (RSD) for ten approved measurements was 3.21%, indicating a good sensing reproducibility. The stability of the Catalase immobilized CPE/ZnS Nps was also examined. For determination of 5 μM bilirubin, no major decrease in current response was found in the 14 days. Only about 4.7% decrease found after 35 days. An 87% current response was quiet retained after 75 days. The reproducibility and stability in this research is better than other similar works [60, 70, 71]. Therefore, the stability of the proposed bilirubin biosensor was good enough for medical operation.

4. CONCLUSION

In this study, we have shown the important and cheap method for bilirubin detection. The Catalase immobilized CPE/ZnS Nps could fast transfer electron and provide good chemical signals for transducer. The constructed bilirubin biosensor exhibited a high sensitivity, fast amperometric response, low detection limit, wide linear dynamic range, high anti-interferent, good reproducibility

and stability. These results demonstrate that ZnS Nps is an attractive material for the fabrication of efficient Nano based biosensors. Also the fast electron transfer frequency and excellent catalytic capability to the oxidation of bilirubin to biliverdin showed that the catalase retains its bioactivity fine.

ACKNOWLEDGEMENT

This research was supported by Lexis Academy (UAE, Iran).

References

1. A. McDonagh, *Clinics in perinatology*, 17 (1990) 359.
2. T. W.Sedlak, and S.H. Snyder, *Pediatrics*, 113 (2004) 1776.
3. K. Weinbren, and B.H. Billing, *British journal of experimental pathology*,. 37 (1956) 199.
4. M.T. Long, and L.S. Friedman, *Hepatic structure and function*. Gastrointestinal Anatomy and Physiology: The Essentials, (2014).
5. R. Lu, and X.L. Zheng, *Blood*, 124 (2014) 2882.
6. P.N. Hopkins, et al., *Arteriosclerosis, thrombosis, and vascular biology*,. 16 (1996) 250.
7. L.Vitek, et al., *Atherosclerosis*, 160 (2002) 449.
8. K. Chan, et al., *Diabetologia*, 56 (2013) 724.
9. E. Lang, et al., *Hepatology*, 61(2015) 275.
10. L. Tolosa, et al., *Liver Transplantation*, 21 (2015) 801.
11. A. Aslihan Avan, S. Aydar, and H. Filik, *Current Analytical Chemistry*, 11 (2015) 96.
12. Zhu, C., et al., *Analytical chemistry*, 7 (2015) 2479.
13. I. Palchetti, and M. Mascini, *Electrochemical Biosensors* (2015).
14. E. Kuposova, et al., *Sensors and Actuators B: Chemical*, 207 (2015) 1045.
15. B. Shoham, et al., *Biosensors and Bioelectronics*, 10 (1995) 341.
16. J. Wang, and M. Ozsoz, *Electroanalysis*,. 2 (1990) 647.
17. X. Li, and Z. Rosenzweig, *Analytica chimica acta*,. 353 (1997) 263.
18. B. Batra, et al., *Biosensors and Bioelectronics*, 44 (2013) 64.
19. Cordeiro, C., et al., *Biosensors and Bioelectronics*, 67 (2015) 677.
20. F. Bettazzi, et al. in *AISEM Annual Conference, 2015 XVIII*. IEEE (2015).
21. Y. Zhou, et al., *Analytica chimica acta*, 840 (2014) 28.
22. J.-H. Kim, et al., *Sensors and Actuators B: Chemical*, 197 (2014) 20.
23. A. Simonian, in *2014 ECS and SMEQ Joint International Meeting*. Ecs (2014).
24. O. Syshchyk, et al., *Biosensors and Bioelectronics*, 66 (2015) 89.
25. R. Angeloni, et al., *Current Analytical Chemistry*,. 11(2015) 56.
26. N. Lončar, and M.W. Fraaije, *Applied microbiology and biotechnology*,. 99 (2015) 3351.
27. A. Trifonov, et al., *Advanced Energy Materials*, (2015).
28. P. Calandra, M. Goffredi, and V.T. Liveri, *Colloids and Surfaces A: Physicochemical and Engineering Aspects*,. 160 (1999) 9.
29. M. Wang, et al., *Solid State Communications*, 115 (2000) 493.
30. A. Mnyusiwalla, A.S. Daar, and P.A. Singer, *Nanotechnology*,. 14 (2003) 9.
31. M.P. Hughes, *Nanotechnology*,. 11 (2000) 124.
32. E. Katz, I. Willner, and J. Wang, *Electroanalysis*, 16 (2004) 19.
33. R. Bandaranayake, et al., *Applied physics letters*, 67 (1995) 831.
34. X. Cheng, M. Filiaggi, and S.G. Roscoe, *Biomaterials*, 25 (2004) 5395.
35. J.S. Griffith, Cambridge University Press (1961).
36. B. Andonovic, et al., *Journal of Chemical Technology and Metallurgy*, 49 (2014) 545.
37. B.A. Prakasam, et al., *Materials Letters* (2015).

38. P.T. Nga, et al., *International Journal of Nanotechnology*, 12 (2015) 525.
39. A. Ricci, et al., *Physical Review B*, 84 (2011) 060511.
40. K.H. Lim, et al., *Advanced Materials*, 25 (2013) 2994.
41. L. Priya, *Mapana-Journal of Sciences*, 12 (2013) 31.
42. U. Raghavan, B. ANKAMWAR, and M. Sastry, *Luminescence Of ZnS Nanoparticles In Organic Phase And Effect Of Doping* (2014).
43. H. Zhang, et al., *ACS nano*, 6 (2012) 4349.
44. R. Rusdi, et al., *Powder Technology*, 210 (2011) 18.
45. L.E.F. Torres, S. Roche, and J.-C. Charlier, *Introduction to graphene-based nanomaterials: from electronic structure to quantum transport*. Cambridge University Press (2014).
46. A. Khan, S. Ganji, and S.N. Mohammad, in *Toward Quantum FinFET*, Springer, (2013) 25.
47. J.I. Goldstein, et al., *materials scientists, and geologists*. Plenum Publishing Corporation (1981).
48. D.C. Joy, *Scanning electron microscopy*. Materials Science and Technology, (1971).
49. C.V. Mun'delanji, et al., *Nanobiosensors and Nanobioanalyses*, Springer (2015).
50. E. Morales-Narváez, and A. Merkoçi, *Medical Nanobiosensors*, Springer (2014).
51. X. Zhang, et al., *Biosensors and Bioelectronics*, 52 (2014) 281.
52. M. Negahdary, et al., *Advances in Environmental Biology*, 6 (2012) 1095.
53. M. Negahdary, *Advances in Environmental Biology*, 5 (2011) 3241.
54. G. Mohseni, et al., *Int J Electrochem Sci*, 7(2012) 12098.
55. Y. Zeng, et al., *Electrochimica Acta*, 130 (2014) 504.
56. E. Laviron, *Journal of Electroanalytical Chemistry and Interfacial Electrochemistry*, 101(1979) 19.
57. H. Kalita, et al., *Applied Nanoscience*, 2015 (2015) 1.
58. P.S. Dorraji, and F. Jalali, *Bioelectrochemistry*, 101 (2015) 66.
59. C. Medina-Plaza, et al., *Analytica chimica acta*, 851 (2014) 95.
60. M.A. Rahman, et al., *Biosensors and Bioelectronics*,. 23 (2008) 857.
61. I. Taurino, et al., *Talanta*, 130 (2014) 423.
62. I. Taurino, et al., *Thin Solid Films*, 548 (2013) 546.
63. M. Silvestrini, et al., *Electrochimica Acta*, 147 (2014) 401.
64. Klemm, J., M.I. Prodromidis, and M.I. Karayannis, *Electroanalysis*, 12 (2000) 292.
65. N.A. Turner, and E.N. Vulfson, *Enzyme and microbial technology*, 27 (2000) 108.
66. R.K. Scopes, *Clinica chimica acta*, 237 (1995) 17.
67. P. Hochachka, and G. Somero, *Comparative biochemistry and physiology*, 27 (1968) 659.
68. J. Hawker, and C. Jenner, *Functional Plant Biology*, 20 (1993) 197.
69. T.J. Roussel, et al., *Amperometric Techniques*, Springer (2014).
70. S. Brocato, C. Lau, and P. Atanassov, *Electrochimica Acta*, 61 (2012) 44.
71. R. Holze, *CMA Brett, AMO Brett: Oxford University Press*, Oxford (1993).